

INTER-ACTIVE REGION CONNECTION OF SYMPATHETIC FLARING ON 2000 FEBRUARY 17

HAIMIN WANG, JONGCHUL CHAE, VASYL YURCHYSHYN, GUO YANG, MICHAEL STEINEGGER, AND PHILIP GOODE
Big Bear Solar Observatory, New Jersey Institute of Technology, 40386 North Shore Lane, Big Bear City, CA 92314-9672;
haimin@flare.njit.edu

Received 2001 February 19; accepted 2001 May 30

ABSTRACT

We have analyzed high-resolution $H\alpha$ full disk data from Big Bear Solar Observatory (BBSO); magnetograph and EUV data from the Michelson Doppler Imager, Large Angle and Spectrometric Coronagraph, and Extreme Ultraviolet Imaging Telescope on board *SOHO*; and *Yohkoh* soft X-ray data of 2000 February 17. Two sympathetic M-class solar flares erupted in succession in NOAA Active Region 8869 and 8872, respectively. The eruption from AR 8872 was followed by an extremely symmetric halo coronal mass ejection (CME). We demonstrate the loop activation, which appears to be the consequence of the first flare in AR 8869 and the cause of the second flare in AR 8872. The activation started in the form of a surge just after a filament eruption and its associated flare in AR 8869. The surge quickly turned into a set of disturbances that propagated at a speed of about 80 km s^{-1} toward the other active region AR 8872. The second flare followed in less than an hour after the arrival of the disturbances at AR 8872. The moving disturbances appeared in absorption in both $H\alpha$ and EUV 195 Å images. The disturbances may represent mass transfer, which had a significant velocity component perpendicular to the field lines and, hence, caused the transport of field lines. In this case, the disturbances may be considered to be a special kind of surge, which we may call a “sweeping closed-loop surge.” We also demonstrated large area dimmings associated with the CME in three active regions. The dimming started from AR 8869 and AR 8872 and was extended to AR 8870, which was on the opposite side of the solar equator. We believe that both the activation of inter-active region loops and the large-scale dimming are the signatures of large-scale restructuring associated with the CME.

Subject headings: Sun: activity — Sun: coronal mass ejections (CMEs) — Sun: flares — Sun: magnetic fields

1. INTRODUCTION

A solar coronal mass ejection (CME) represents a large-scale rearrangement of the Sun’s magnetic structure, which can lead to a coronal transient in the interplanetary medium. Each CME may carry away a mass of up to 10^{13} kg and release up to 10^{25} J of energy from coronal magnetic fields (Harrison 1991, 1995, and 1997). CMEs have been studied using a number of coronagraphs since the 1970s, e.g., *Skylab*, *Solwind*, and *SMM*. Filament eruptions and solar flares may be local events that are associated with CMEs, however, the specific connection remains to be established. The launch of a new generation coronagraph—the Large Angle and Spectrometric Coronagraph (LASCO) on board *Solar and Heliospheric Observatory (SOHO)*; Domingo, Fleck, & Poland 1995—provides the most advanced tool to study the dynamics of coronal structures (Brueckner et al. 1995). LASCO comprises three coronagraphs (C1, C2, and C3), extending from 1.1 to 30 solar radii. The white-light instruments (C2 and C3) not only provide excellent observations of limb CME events, but also have the sensitivity to detect the “halo” from the disk events after the CME material moves beyond the edge of the occulting disk. A halo event was first reported by Howard, Michels, & Sheeley (1982), using observations made with the *Solwind* coronagraph on the *P78-1* spacecraft. Several halo events were studied based on LASCO observations (Plunkett et al. 1998, Thompson et al. 1998; Zarro et al. 1999). Halo events (including “partial” halo events) appear more important in space weather than disk events, since they are related to the Earth-directed CMEs.

Disk coronal dimmings have been identified in association with halo events detected with the *Yohkoh* Soft X-ray

Telescope (SXT; Tsuneta et al. 1991) and *SOHO* Extreme Ultraviolet Imaging Telescope (EIT; Delaboudinière et al. 1995), e.g., Gopalswamy & Hanaoka (1998), Sterling & Hudson (1997), and Thompson et al. (1998). Those transient dimmings are often interpreted to represent the loss of the coronal mass which is swept into the CMEs. Wang et al. (2000) found that for the eruptions studied, the onset of dimming occurred hours before the onset of the associated flares. Therefore, flares might represent only a small part of the larger scale restructuring of magnetic fields that caused CMEs.

The large-scale structure is an important issue which received much attention recently in relation to the CME mystery. One kind of phenomenon associated with the large-scale structure is the so-called sympathetic flares (Gopalswamy et al. 1999; Shi, Wang, & Luan 1997; Pearce & Harrison 1990), which are consecutive flares occurring in nearby active regions, during a short period of time. Another kind of large-scale structure receiving attention is transequatorial loops (Pevtsov 2000), which connect two active regions in opposite hemispheres. Khan & Hudson (2000) discussed a flare launching a “shock” from one active region to another, during the homologous sudden disappearance of transequatorial loops. Each of the disappearances was closely associated with a flare and a CME. It is important to find out different kinds of interactions between active regions and related initiation of CMEs.

In the present paper, we report a pair of sympathetic flares in NOAA Active Region 8869 and 8872 that were connected by an activation of inter-active region loops, as seen primarily in full disk $H\alpha$ data taken at Big Bear Solar Observatory (BBSO). At the end of 1995, BBSO started its

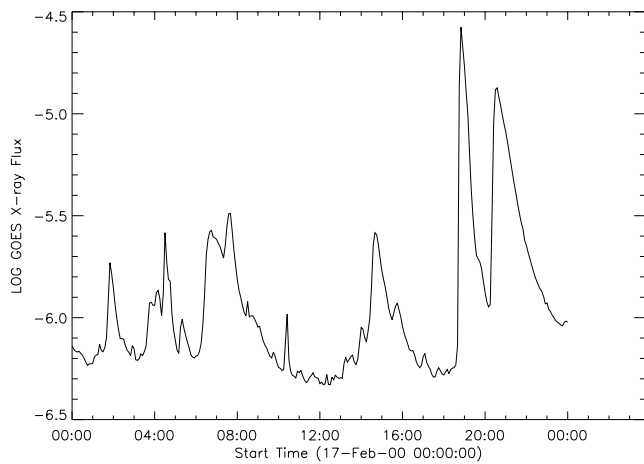


FIG. 1.—GOES X-ray plot showing the lower energy channel (1–8 Å) time and magnitude of two M-class flares. The M2.5 flare occurred in AR 8869, started at 1841 UT, and peaked at 1852 UT; the M1.3 flare occurred in AR 8872, started at 2017 UT, and peaked at 2035 UT.

new generation of full disk $H\alpha$ observations (Denker et al. 2000). Every minute a full disk $H\alpha$ image is recorded by a 2048×2048 Kodak 8 bit Megaplug camera with the 8 inch Singer-Link telescope. The pixel size of the images is roughly $1''$, which yields a spatial resolution of $2''$. Owing to BBSO's long-lasting clear skies and good seeing conditions, these movies provide a unique tool to monitor solar activity on the scale of the full disk and, thereby, enabling one to study the large-scale structures of flares. Our $H\alpha$ operation has been extended to a three-station network (BBSO, Kanzelhoehe Solar Observatory in Austria, and Yunnan Observatory in China; Steinegger et al. 2000).

2. OBSERVATIONS AND DATA REDUCTION

For our current study, the data are from the following sources:

1. BBSO full disk $H\alpha$ movies. As we described above, the cadence was 1 minute and the pixel resolution was $1''$. The observations well covered both the flares.

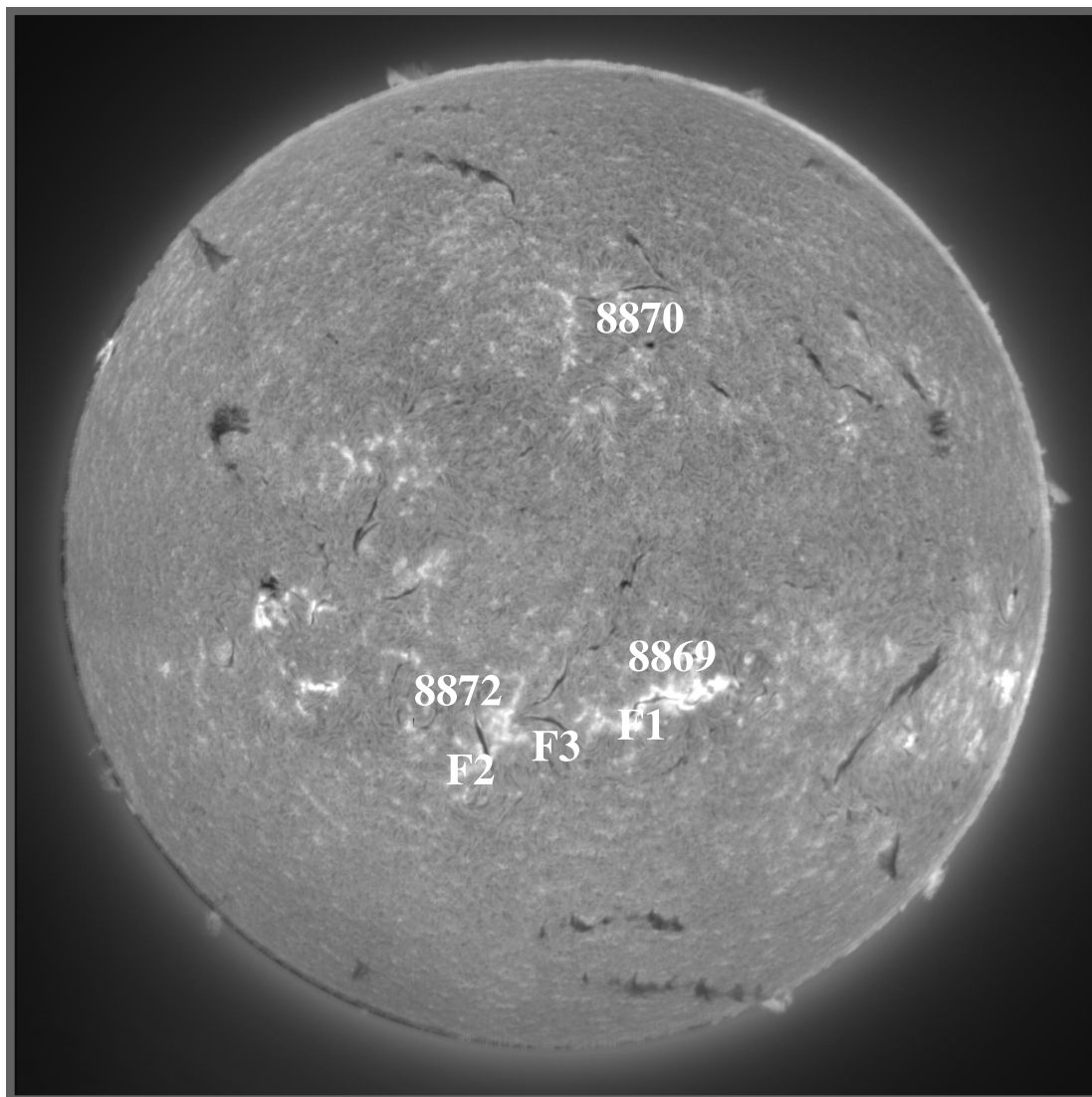


FIG. 2.—Full disk $H\alpha$ data at 1800 UT. F1, F2, and F3 are three filaments. Three active regions are marked on the figure.

2. EIT Fe XII 195 Å full disk movies. EIT provides wide-field images of the corona and transition region on the solar disk and up to 1.5 solar radii above the solar limb. It observes in four spectral lines: Fe IX (171 Å), Fe XII (195 Å), Fe XV (284 Å) and He II (304 Å). These lines allow imaging of solar plasma at certain temperature diagnostics in the range 6×10^4 K to 3×10^6 K (Delaboudinière et al. 1995). On 2000 February 17, only Fe XII 195 Å data were obtained continuously. The sensitivity of this line peaks between 1 and 2 MK. Cadence was 15 minutes, and pixel resolution was 2".

3. LASCO coronagraph data. We are especially interested in the C2 and C3 white-light data for CMEs. C2 and C3 are two externally occulted instruments. C2 covers the range of 2 to 6 solar radii, and C3 covers 4 to 32 solar radii (Brueckner et al. 1995). The cadence for our data was 24 minutes.

4. Full disk Michelson Doppler Imager (MDI) magnetograms. MDI mainly obtains full-disk Dopplergrams, for the investigation of solar oscillations. However, it can obtain magnetograms of various cadences and image sizes (Scherrer et al. 1995). For the data used in the current study, the cadence was 90 minutes, and the pixel size was 2".

5. *Yohkoh* Soft X-ray data. SXT is an instrument on board *Yohkoh* to study thermal structure of solar plasma (Tsuneta et al. 1991). For the two events analyzed in this paper, full disk *Yohkoh* SXT images were obtained in three filters (A11, A12, and A1Mg, which cover a wide temperature range from 3 to 10 MK). Unfortunately, only a few images were observed covering both of the flares.

As all the data are full disk images, the alignments were very easy. We find the center and radius of each image by

limb fitting and make rotational adjustment by visual inspection.

3. RESULTS

3.1. General View of the Inter-active Region Connection

Figure 1 shows the *GOES* lower energy channel (1–8 Å) soft X-ray light curve of 2000 February 17. Figure 2 shows a BBSO H α full disk image before the two events, with active region numbers marked. The M2.5 flare occurred in AR 8869, started at 1841 UT, and peaked at 1852 UT; the M1.3 flare occurred in AR 8872, started at 2017 UT, and peaked at 2035 UT. Based on the closeness in both space and time of the two events, we can classify them as sympathetic flares. Both the active regions did not have complicated magnetic field configuration, both had a filament (F1 and F2, respectively). There is a third filament (F3) between these two active regions. Based on magnetic topology, we found that the filament F2 is dextral, whereas F1 and F3 are sinistral (Martin 1998). AR 8870 is a much decayed active region.

Figure 3 demonstrates the sequence of the events from a subarea of the full disk H α data: 1801 UT: preflare state, all three filaments were well visible; 1851 UT: F1 disappeared and the M2.5 flare was in progress; 1917 UT: the loop structure appeared above F3, but F3 remained the same throughout the observations; and 2024 UT: F2 disappeared and the M1.3 flare was in progress. The second event occurred in AR 8872, which has a typical sigmoid configuration (Canfield, Hudson, & McKenzie 1999). If we view the two flare events separately, each of them looks like a relatively simple two-ribbon flare. The two flares, however, seemed to be causally connected to each other as seen from

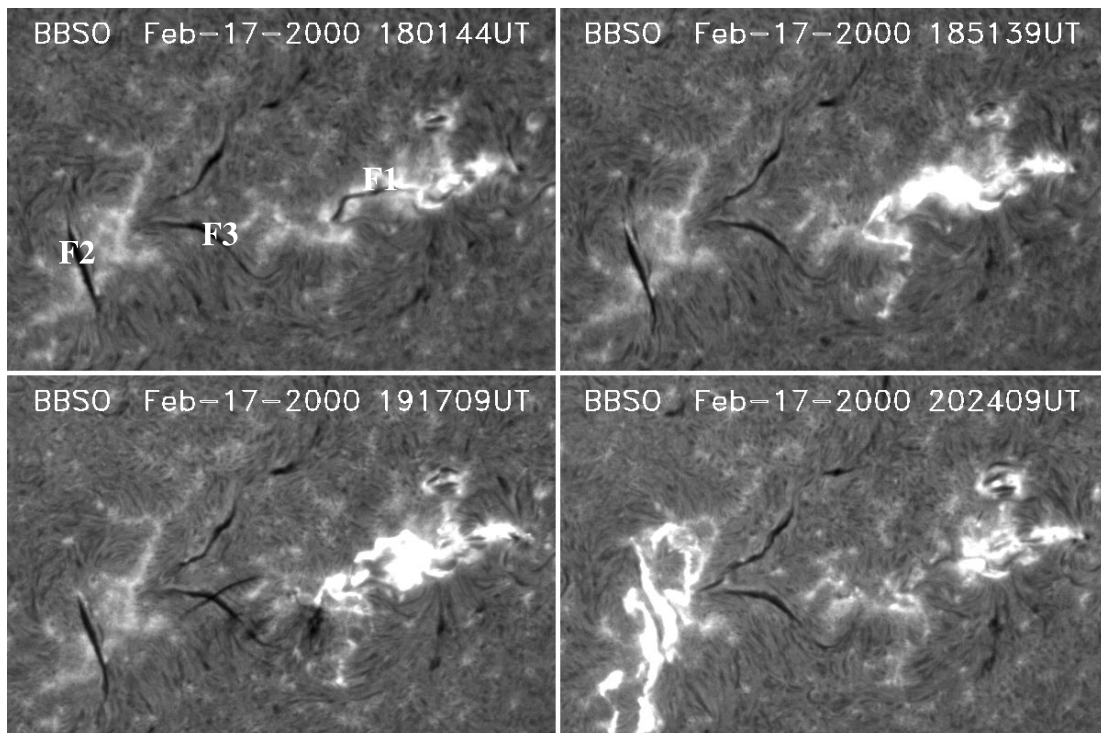


FIG. 3.—Sequence of H α images from BBSO full disk to show the evolution of the active regions during the process of two flares and filament eruptions. The field of view is $600'' \times 400''$.

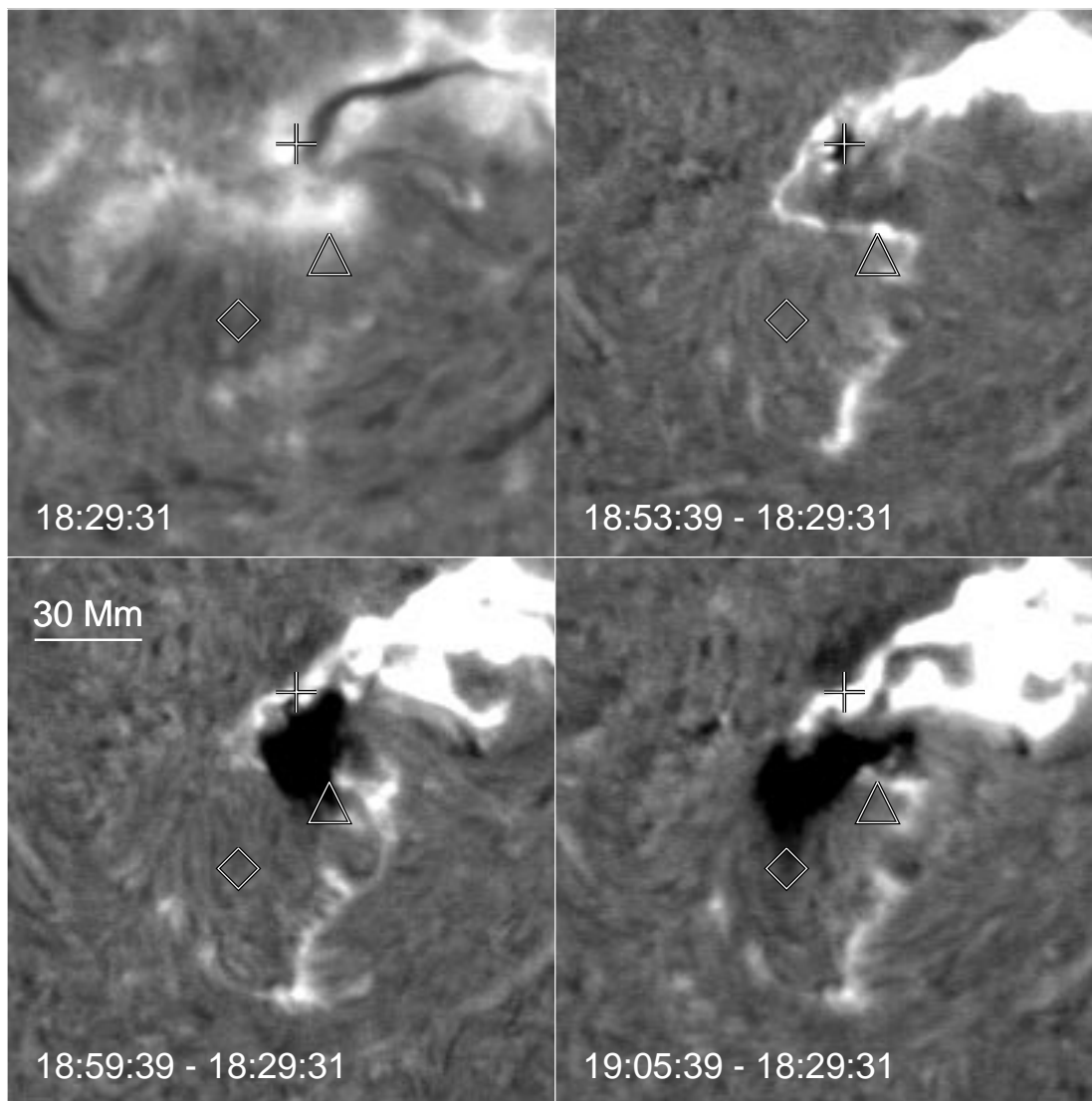


FIG. 4.—Early sequence of H α images showing the start of the surge. The inferred positions of the surge front at the three instants are marked by the symbols. The surge displays not only the outward ejection, but also the clockwise rotation. The first image is a preflare image at 182931 UT, and all other images were subtracted by this preflare image.

the archlike moving disturbances that are visible in the frame of 1917 UT, although we could not exclude the possibility of coincidence. These disturbances provided a critical link between the two active regions and two flares, and are the central issue of this paper.

3.2. Evolution of the H α Disturbances

Figure 4 shows the initial development of a surge that is associated with the first flare in AR 8869. The last three images were subtracted by the first image (preflare image). The starting point is marked by the plus sign. It is very close to one end of the filament F1, so the surge may be related to the eruption of this filament—part of the material in F1 may be swept to the surge. The surge initially moves a distance of about 34,000 km to the southwest for 6 minutes (to the point of the triangle, in the 18:59:39 panel), so its speed is inferred to be 94 km s^{-1} . It changes its direction southeast during the next 6 minutes (to the point of the diamond, in the 19:05:39 panel). This indicates that the

surge involves a clockwise rotation as well as the jetlike ejection. The speed of the surge during this time interval is about 83 km s^{-1} .

The next evolution stage of the surge is shown in Figure 5. With the rotation and outward ejection, the surge begins to display filamentary structures labeled “a,” “b,” and “c.” But these structures soon fade away. Meanwhile, new structures, labeled “1” and “2,” emerge. These moving disturbances are different from the other structures in that they are faint initially, but later become distinct. The location of the disturbance 1 at each instant is marked by a curve. All the locations of the disturbance 1 at the four instants are indicated over the image taken at 19:18:39 UT. Its propagation speed is estimated to be about 78 km s^{-1} . The second disturbance (2) follows the first one with a separation of about 40,000 km between the two. Note that its first identified location at 19:12:39 UT is much away from the surge. This is the most confusing part of the evolution of the eruption. Structures 1 and 2 might be continuations of mass

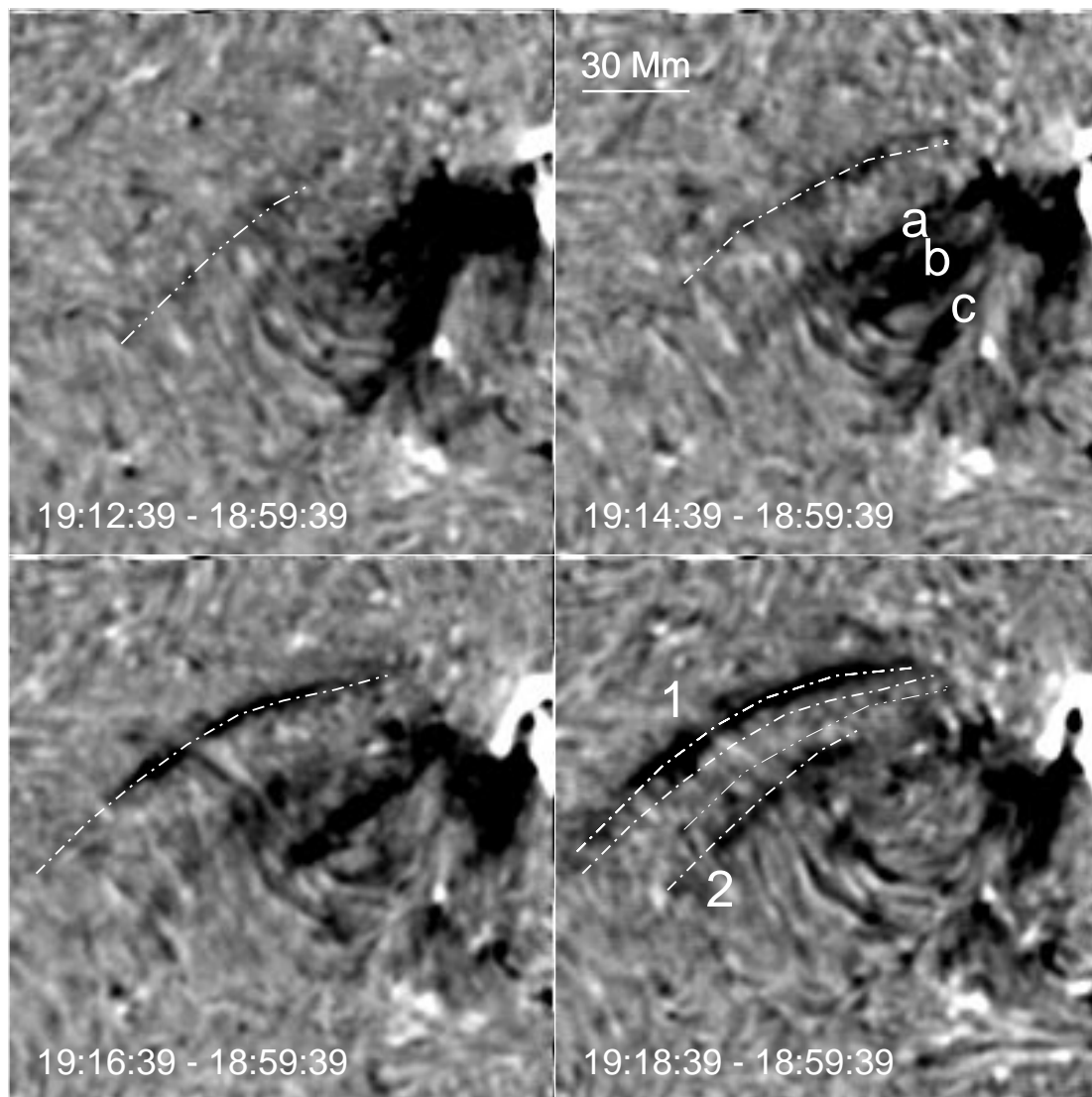


FIG. 5.—Intermediate sequence of $H\alpha$ images showing the development of the moving disturbance. The surge displays the filamentary structures (a, b, and c) which soon fade away. There are two moving disturbances, labeled “1” and “2.” The locations of the first disturbance at different instants are represented by the different curves. All the images were subtracted by an image at 185939 UT to enhance the visibility of the disturbances.

motions of a, b, and c, moving in a northeast direction, and we lost the track of the link due to insufficient temporal resolution.

Figure 6 shows the final stage of the moving disturbances. They become noticeably broadened with the slowdown of propagation. The propagation speed is now about 42 km s^{-1} . The north portions of the fronts move more slowly than the southwest portions. This difference in the propagation speed results in the distortion of the shapes of the moving disturbances, especially the second one. Finally, the two disturbances are disrupted and disappear in $H\alpha$.

3.3. Comparison with EIT 195 Å Images

Figure 7 shows the EUV images at 195 Å taken by SOHO/EIT. The $H\alpha$ disturbances 1 and 2 are overplotted as two prominent white dashed lines. The EUV images clearly show the distinct absorption features that could be identified with the moving disturbances seen in $H\alpha$. They have propagation speeds comparable to those inferred from the

$H\alpha$ images. The disturbances seen in the EUV wavelength, however, are slightly different from their $H\alpha$ counterparts in a couple of ways. First of all, they are not exactly cospatial with, but follow behind their $H\alpha$ counterparts. This difference cannot be explained by a slight difference in observing time. Moreover, they are darker at 19:11:58 UT than at 19:24:16 UT, whereas the opposite is true for their $H\alpha$ counterparts. These differences suggest that the moving disturbances have complicated thermodynamic structures.

3.4. Magnetic Configuration

The evolution of the magnetic field structure would provide important clues on the physical picture of the above described events. The only available time sequence magnetograms were from MDI. Figure 8 shows the constant α linear force-free field extrapolation of an MDI line-of-sight magnetogram (Abramenko & Yurchyshyn 1996). This was done by choosing $\alpha = 0.0075 \text{ arcsec}^{-1}$ to match the pre-eruption *Yohkoh* soft X-ray loop structure (Yurchyshyn et

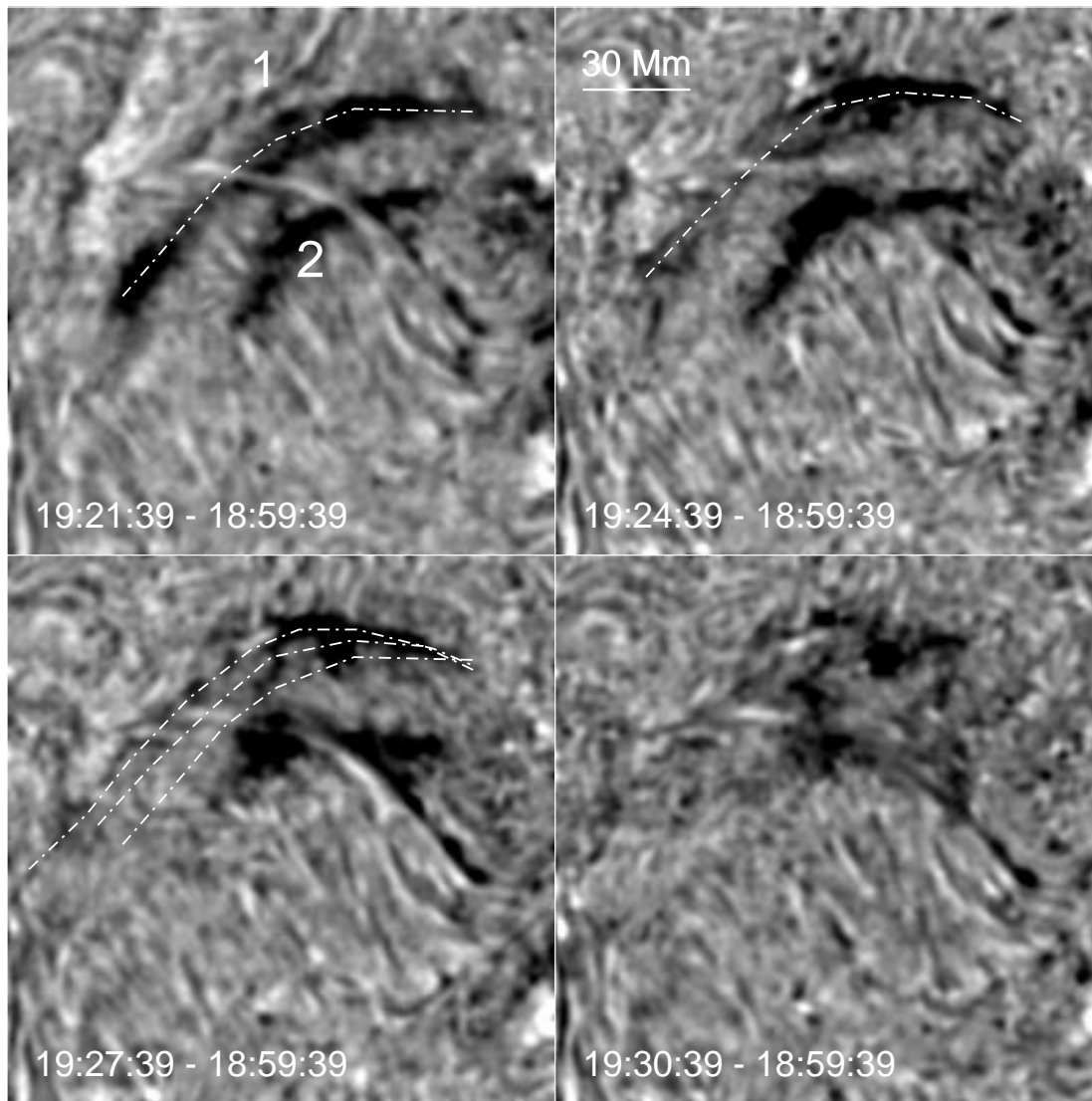


FIG. 6.—Later sequence of H α images showing the disappearance of the moving disturbance. Again, all the images were subtracted by an image at 185939 UT to enhance the visibility of the disturbances.

al. 2000). Two types of extrapolated field lines are connected near the base where the surge appeared—open field lines and closed field lines connecting two active regions. We believe that the open field lines prescribed the configuration for the appearance of the surge in the first stage, and the closed field lines prescribed the magnetic configuration of moving disturbances of loops, which linked two active regions. Magnetic flux cancellation was seen at the base of the surge.

Two field systems seem to exist around the filament F3. One is a set of field lines along the filament in the lower atmosphere (chromosphere) as seen from the alignment of H α fibrils around F3. The other is a set of much higher field lines perpendicular to the filament in the upper atmosphere (corona) as seen from the extrapolated field lines and the structures seen in EUV images. The arch-shaped disturbances are located almost perpendicular to the filament and along the coronal field lines. On the other hand, their moving direction is along the chromospheric field lines and across the coronal field lines.

Figure 9 shows the soft X-ray evolution of these two active regions in the process of the two flares. Before the first flare, two regions were connected by a group of short loops (L1), and after the flares, they were connected by much longer loops (L2). L1 may be coronal counterparts of the chromospheric loops which were activated between occurrence of the two flares.

3.5. Large-scale EUV Dimming

Figure 10 shows the EIT 195 Å differencing images (between 182410 UT and 212410 UT). The dimming appears to be extensive around both regions (D1 and D2 in AR 8869; D3 and D4 in AR 8872), and also across the equator to connect a decayed active region (D5 in AR 8870). We observed that the dimming occurred first in AR 8869 and then 8872, and then was propagating from AR 8872 to AR 8870, crossing the equator. We believe that the CME is associated with these five dimming areas. The large-scale dimming of this event explained the morphology of the CME as seen in LASCO/C2 and C3: even though the

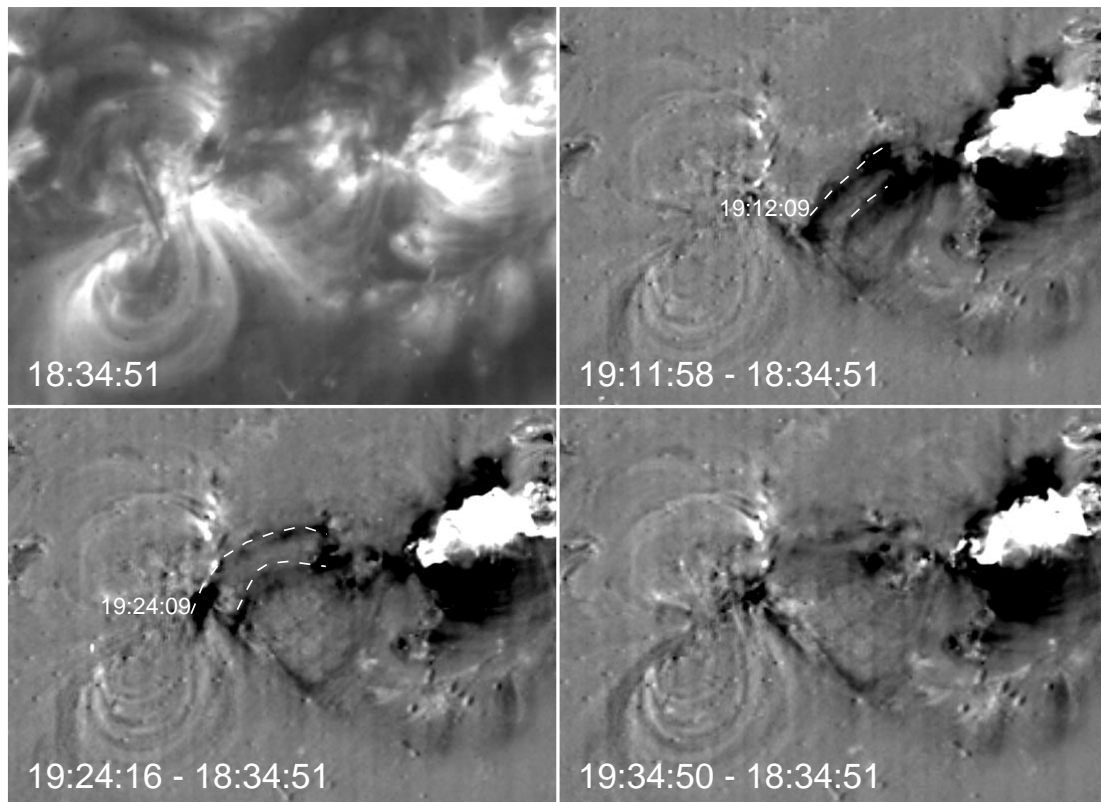


FIG. 7.—EIT 195 Å images showing the evolution of the moving disturbances. The curves at each instant represent the locations of the two disturbances as seen in H α .

source AR (AR 8872) is located in the southeast of the disk, the halo CME was extremely isotropic.

4. DISCUSSIONS

We have described activation of inter-active region loops:

loops connecting two active regions which appear to link two sympathetic flares. This activation seems to have triggered the flare activity of the second active region. The loop activation started with a surge in an open field area and then activated the closed loops. The surge that started from

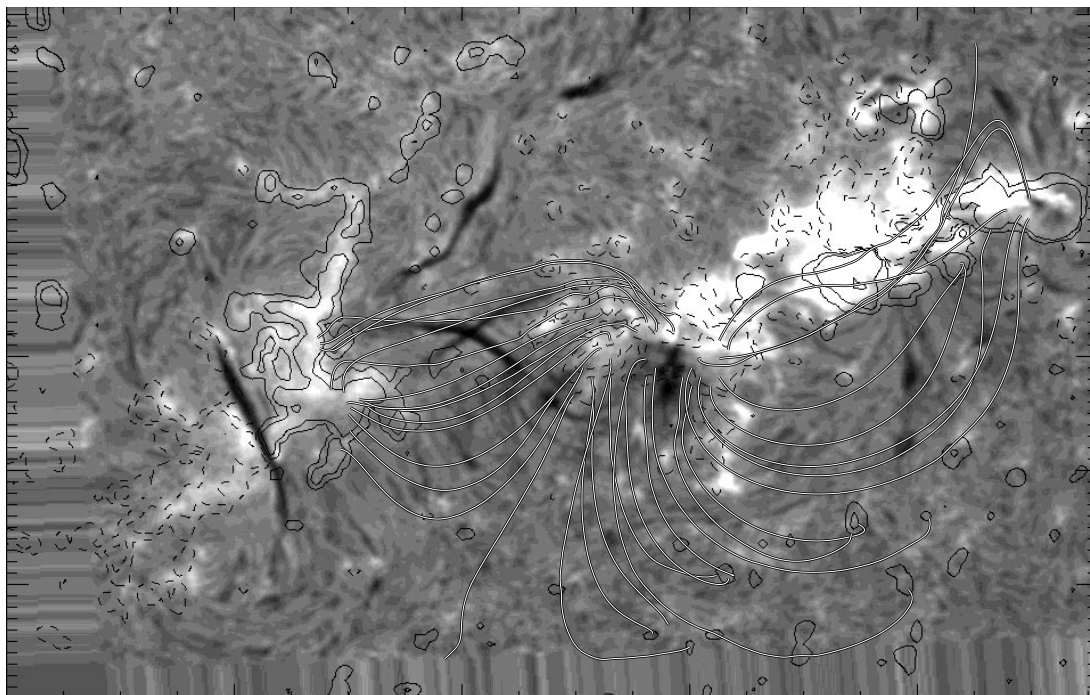


FIG. 8.—Background: H α image at 1917 UT. Contours: MDI magnetogram at 1735 UT showing positive polarity (*solid contours*), negative polarity (*dashed contours*), and the result of constant α linear force-free extrapolation (*lines*).

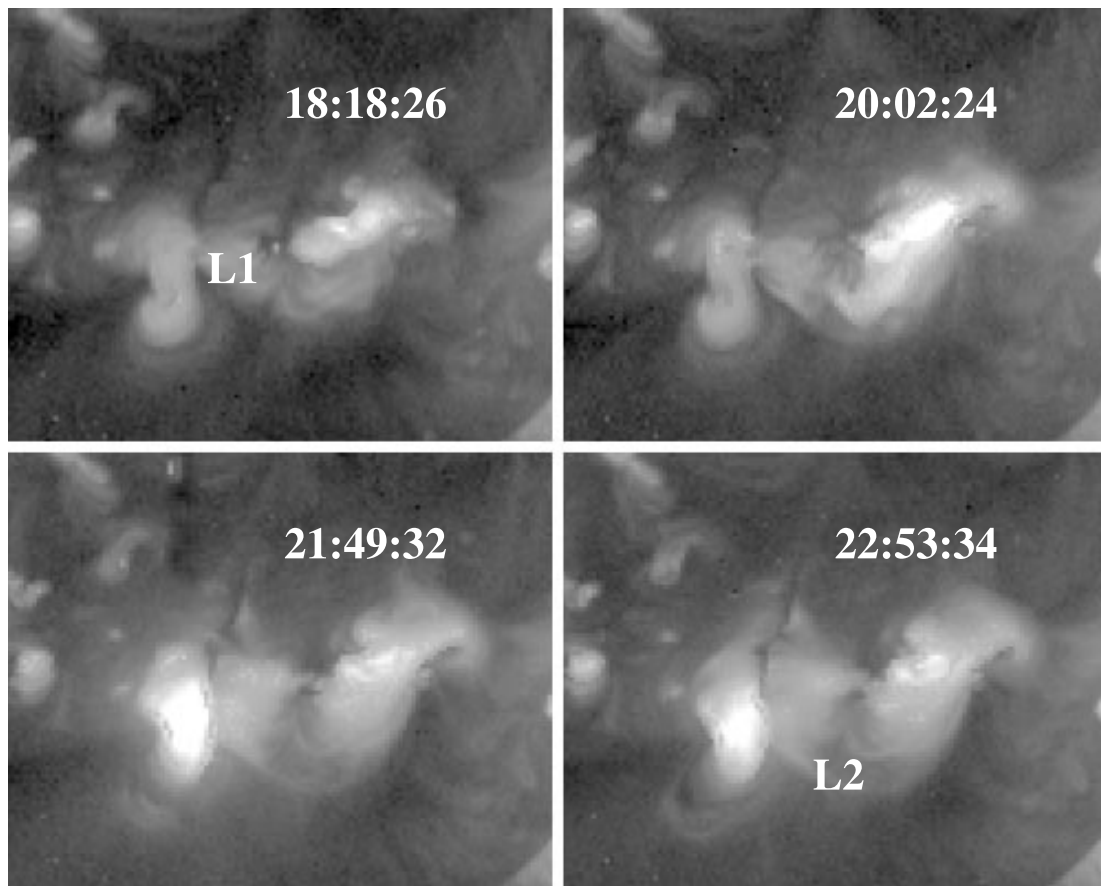


FIG. 9.—Evolution of soft X-ray structure before, between, and after the two flares. The images were from full disk *Yohkoh* SXT data. The field of view is $625'' \times 500''$.

the first active region turned into H α and EUV absorption disturbances that moved toward the second active region. Both open and closed loop structures are confirmed by linear force-free extrapolation of magnetic fields (Fig. 8). The large-scale structure of the events was further demonstrated by the dimming being spread over rather large areas covering three active regions. Our finding is consistent with, but more elaborate than, the previous result of Harrison (1995) that CME source region is commonly much larger than the active region, which can be on one leg of a CME.

It is interesting to note the mass transports related to several sequential events. Part of the mass from the first filament eruption in NOAA AR 8869 became part of the mass in the surge in one end of the active region. The mass is somehow trapped in the closed loops adjacent to the surge. Then the mass motion was observed from NOAA AR 8869 to NOAA AR 8872. One of the possible consequences is that the material in NOAA AR 8872 is more than what is needed to balance the magnetic tension, an instability occurred to trigger the second flare/filament eruption and CME. Finally, the dimmings in the three active regions are clearly associated with the mass in the halo CME.

Previous studies on sympathetic flares only described the closeness in time and space. This study provides evidence that there might be interaction and mass transport between two source regions. This needs to be studied further by high-cadence, high-resolution full disk observations, such as observations from the Global H α Network, lead by BBSO (Steinberger et al. 2000).

The observed moving disturbances were interpreted as motion of flux tubes. Loops disappeared due to the decrease in the density as the loops rise. However, it could have another interpretation: the propagation of compression waves, generated by the high-speed perturbation due to the surge. If the disturbances are due to waves, they may be of a different kind than Moreton waves or EIT waves since the observed propagation speed is much lower than that of Moreton or EIT waves. Smith & Harvey (1971) studied Moreton wave or “flare wave” transients, and they stated that a large number of the propagating disturbances can appear dark in H α images, as if cool material is moving. However, they indicated that these disturbances are typically arc-shaped and are centered about the flare. For the case studied here, the surge appears to be the origin, southeast of the flaring area. The multiple fronts, speed, propagation direction, and also the darkness indicate that these are different from Moreton waves. The disturbances might be fast shocks propagating through a rather cold medium where the Alfvén speed is much greater than the sound speed. If so, the Alfvén speed must be close to the propagation speed of the disturbances. This may constrain the magnetic field of the propagating medium, once the density is determined. If the disturbances are due to waves, their disappearances are likely due to heating by the wave. Several shock fronts may require several triggerings, for which we do not have evidence from the present observations.

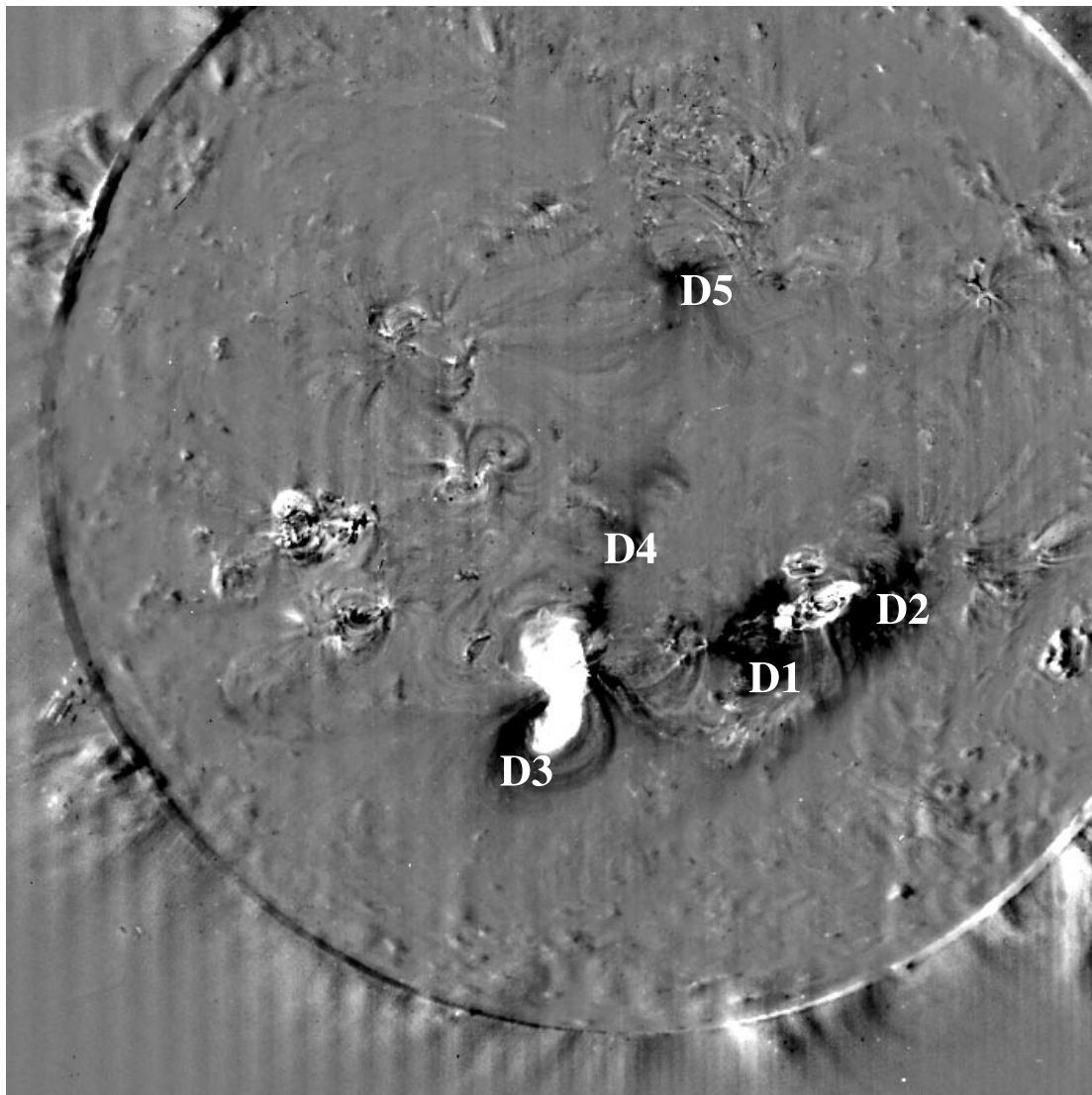


FIG. 10.—Differencing EIT image between 212410 UT and 182410 UT showing dimming areas, which are spread in large areas. D1 and D2 are associated with AR 8869; D3 and D4 are associated with AR 8872; D5 is on the other side of the equator and is at the edge of AR 8870.

We are grateful to the observing staff at BBSO for their support in obtaining the data. We would like to thank the anonymous referee for very helpful comments to improve the manuscript. The work is supported by NSF under

grants ATM-0076602, ATM-9903515 and ATM-0086999, NASA under grants NAG5-9682, NAG5-9738, and NAG5-7085, and ONR under grant N00014-97-1-1037.

REFERENCES

- Abramenko, V., & Yurchyshyn, V. 1996, *Sol. Phys.*, 168, 42
 Brueckner, G. E., et al. 1995, *Sol. Phys.*, 162, 357
 Canfield, R. C., Hudson, H. S., & McKenzie, D. E. 1999, *Geophys. Res. Lett.*, 26, 627
 Delaboudinière, J. P., et al. 1995, *Sol. Phys.*, 162, 291
 Denker, C., Johannesson, A., Marquette, W., Goode, P. R., Wang, H., & Zirin, H. 1999, *Sol. Phys.*, 184, 87
 Domingo, V., Fleck B., & Poland, A. I. 1995, *Sol. Phys.*, 162, 1
 Gopalswamy, N., & Hanaoka, Y. 1998, *ApJ*, 498, L179
 Gopalswamy, N., Nitta, N., Manoharan, P. K., Raoult, A., & Pick, M. 1999, *A&A*, 347, 684
 Harrison, R. A. 1991, *Philos. Trans. R. Soc. London*, A 336, 401
 ———. 1995, *A&A*, 304, 585
 ———. 1997, in *Proc. 31st ESLAB Symp. (ESA SP-415; Noordwijk: ESA)*, 121
 Howard, R. A., Michels, D. J., & Sheeley, N. R., Jr. 1982, *ApJ*, 263, L101
 Khan, J. I., & Hudson, H. S. 2000, *Geophys. Res. Lett.*, 27, 1083
 Martin, S. F. 1998, *Sol. Phys.*, 182, 107
 Pearce, G., & Harrison, R. A. 1990, *A&A*, 228, 513
 Pevtsov, A. A. 2000, *ApJ*, 531, 553
 Plunkett, S. P., Thompson, B. J., Howard, R. A., Michels, D. J., St. Cyr, O. C., Tappin, S. J., Schwenn, R., & Lamy, P. L. 1998, *Geophys. Res. Lett.*, 25, 2477
 Scherrer, P. H., et al. 1995, *Sol. Phys.*, 162, 129
 Shi, Z., Wang, J., & Luan, D. 1997, *Acta Astron.*, 30, 257
 Smith, S. F., & Harvey, K. L. 1971, *Physics of the Solar Corona*, ed. J. Macris (Dordrecht: Reidel), 156
 Steinegger, M., et al. 2000, in *Proc. SOHO 10/GONG Workshop (ESA SP-464; Noordwijk: ESA)*, 617
 Sterling, A., & Hudson, H. S. 1997, *ApJ*, 491, L55
 Thompson, B. J., Plunkett, S. P., Gurman, J. B., Newmark, J. S., St. Cyr, O. C., & Michels, D. J. 1998, *Geophys. Res. Lett.*, 25, 2465
 Tsuneta, S., et al. 1991, *Sol. Phys.*, 136, 37
 Wang, H., Goode, P., Denker, C., Yang, G., Yurchyshyn, V., Nitta, N., Gurman, J. B., & St. Cyr, C. 2000, *ApJ*, 536, 971
 Yurchyshyn, V., Wang, H., Qiu, J., Goode, P. R., & Abramenko, V. I. 2000, *ApJ*, 540, 1143
 Zarro, D. M., Sterling, A. C., Thompson, B. J., Hudson, H. S., & Nitta, N. 1999, *ApJ*, 520, L139